

Rotational symmetry breaking in superconducting nickelate $\text{Nd}_{0.8}\text{Sr}_{0.2}\text{NiO}_2$ films

Haoran Ji^{1#}, Yanan Li^{1#}, Yi Liu^{2#}, Xiang Ding^{3#}, Zheyuan Xie¹, Shichao Qi¹, Liang Qiao^{3*}, Yi-feng Yang^{4,5,6}, Guang-Ming Zhang^{7,8} and Jian Wang^{1,9,10,11*}

¹International Center for Quantum Materials, School of Physics, Peking University, Beijing 100871, China

²Department of Physics, Renmin University of China, Beijing 100872, China

³School of Physics, University of Electronic Science and Technology of China, Chengdu 610054, China

⁴Beijing National Lab for Condensed Matter Physics and Institute of Physics, Chinese Academy of Sciences, Beijing 100190, China

⁵School of Physical Sciences, University of Chinese Academy of Sciences, Beijing 100049, China

⁶Songshan Lake Materials Laboratory, Dongguan, Guangdong 523808, China

⁷State Key Laboratory of Low-Dimensional Quantum Physics and Department of Physics, Tsinghua University, Beijing 100084, China.

⁸Frontier Science Center for Quantum Information, Beijing 100084, China

⁹Collaborative Innovation Center of Quantum Matter, Beijing 100871, China

¹⁰CAS Center for Excellence in Topological Quantum Computation, University of Chinese Academy of Sciences, Beijing 100190, China

¹¹Beijing Academy of Quantum Information Sciences, Beijing 100193, China

[#]These authors contribute equally: Haoran Ji, Yanan Li, Yi Liu and Xiang Ding.

^{*}Corresponding author: jianwangphysics@pku.edu.cn (J.W.), liang.qiao@uestc.edu.cn (L.Q.)

The infinite-layer nickelates, isostructural to the high- T_c superconductor cuprates, have risen as a promising platform to host unconventional superconductivity and

stimulated growing interests in the condensed matter community. Despite numerous researches, the superconducting pairing symmetry of the nickelate superconductors, the fundamental characteristic of a superconducting state, is still under debate. Moreover, the strong electronic correlation in the nickelates may give rise to a rich phase diagram, where the underlying interplay between the superconductivity and other emerging quantum states with broken symmetry is awaiting exploration. Here, we study the angular dependence of the transport properties on the infinite-layer nickelate $\text{Nd}_{0.8}\text{Sr}_{0.2}\text{NiO}_2$ superconducting films with Corbino-disk configuration. The azimuthal angular dependence of the magnetoresistance ($R(\varphi)$) manifests the rotational symmetry breaking from isotropy to four-fold (C_4) anisotropy with increasing magnetic field, revealing a symmetry breaking phase transition. Approaching the low temperature and large magnetic field regime, an additional two-fold (C_2) symmetric component in the $R(\varphi)$ curves and an anomalous upturn of the temperature-dependent critical field are observed simultaneously, suggesting the emergence of an exotic electronic phase. Our work uncovers the evolution of the quantum states with different rotational symmetries and provides deep insight into the global phase diagram of the nickelate superconductors.

The conventional superconductivity with transition temperature (T_c) lower than 40 K was successfully explained by the Bardeen-Cooper-Schrieffer (BCS) theory, in which the electrons with anti-parallel spins and time-reversed momenta form Cooper pairs, and the superconducting order parameter is of isotropic s -wave symmetry^{1,2}. However, the discovery of high-temperature superconductivity ($T_c > 40$ K) in cuprates is beyond the expectation of the BCS theory, and the superconducting order parameters of cuprates are believed to be of nodal d -wave symmetry^{3,4}. Thereafter, the mechanism of unconventional high- T_c superconductivity has become one of the most important puzzles in physical sciences. Recently, the observation of superconductivity in infinite-layer nickelates with a maximal T_c of 15 K in $\text{Nd}_{1-x}\text{Sr}_x\text{NiO}_2$ has motivated extensive

researches in this emerging new superconducting family⁵⁻⁹. Mimicking the d^9 electronic configuration and the layered structure including CuO_2 planes of the cuprates, the isostructural infinite-layer nickelates are promising candidates for high- T_c unconventional superconductivity⁵⁻⁹. Discerning the similarities and the differences between the nickelates and the cuprates, especially in the symmetry of the superconducting order parameters, should be of great significance for understanding the mechanism of unconventional high- T_c superconductivity.

Theoretical calculations have suggested that the nickelates are likely to give rise to a d -wave superconducting pairing, analogous to the cuprate superconductors. However, the consensus has not been reached and there are several proposals, including dominant $d_{x^2-y^2}$ -wave^{10,11}, multi-band d -wave^{12,13}, and even a transition from s -wave to $(d+is)$ -wave and then to d -wave depending on the doping level and the electrons hopping amplitude¹⁴. Experimentally, through the single-particle tunneling spectroscopy, different spectroscopic features showing s -wave, d -wave, and even a mixture of them are observed on different locations of the nickelate film surface, which complicates the determination of the pairing symmetry in the nickelates¹⁵. The London penetration depth of the nickelates family are also measured, and the results on La-based and Pr-based nickelate compounds support the existence of a d -wave component^{16,17}. However, the Nd-based nickelate, $\text{Nd}_{0.8}\text{Sr}_{0.2}\text{NiO}_2$, exhibits more complex behaviors that may be captured by a predominantly isotropic nodeless pairing^{16,17}. The pairing symmetry of the superconducting order parameter in the nickelate superconductors, the fundamental characteristic of the superconducting state, is still an open question, thus further explorations with diverse experimental techniques are highly desired.

In addition to the mystery of the superconducting pairing symmetry, the strong electronic correlation in nickelates is another element that makes the nickelate systems intriguing. The strong correlation is theoretically believed to play an important role in the nickelates systems^{8,9,18,19} and the strong antiferromagnetic (AFM) exchange interaction between Ni spins has been experimentally detected²⁰. Generally, the strong correlated electronic systems are anticipated to host a rich phase diagram and multiple

competing states including superconductivity, magnetic order, charge order, pair density wave (PDW), etc^{21,22}. In the nickelate thin films, the charge order, a spatially periodic modulation of the electronic structure that breaks the translational symmetry, has been experimentally observed by the resonant inelastic X-ray scattering (RIXS)²³⁻²⁵. However, the charge order is only observable in the lower doping regime where the nickelates are non-superconducting. The interplay between the superconductivity and the charge order as well as other underlying symmetry-broken states is still awaiting explorations.

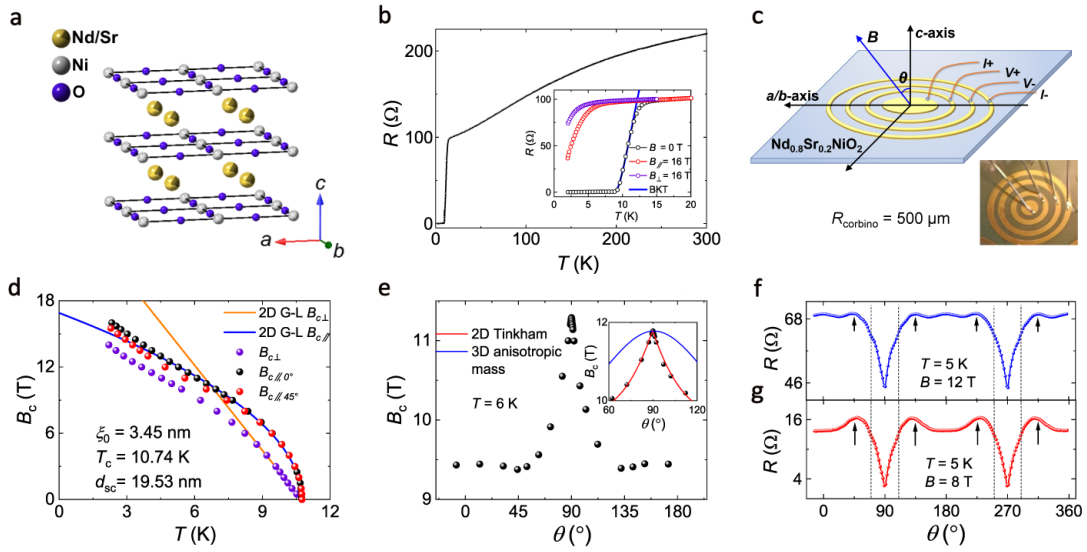


Fig. 1 | Structure and the quasi-two-dimensional superconductivity in $\text{Nd}_{0.8}\text{Sr}_{0.2}\text{NiO}_2$. **a**, Crystal structure of the infinite-layer nickelate $\text{Nd}_{0.8}\text{Sr}_{0.2}\text{NiO}_2$. **b**, Temperature dependence of the resistance $R(T)$ at zero magnetic field from 2 K to 300 K. The inset shows the $R(T)$ curves below 20 K at 0 T (black circles), $B_{//} = 16$ T (red circles), and $B_{\perp} = 16$ T (purple circles). Here, the $B_{//}$ is applied along the a/b -axis and B_{\perp} is along the c -axis. The blue solid line represents the BKT transition fitting using the Halperin-Nelson equation. **c**, Schematic image and optical photo (inset) of the Corbino-disk configuration for polar (θ) angular dependent magnetoresistance $R(\theta)$ measurements on the $\text{Nd}_{0.8}\text{Sr}_{0.2}\text{NiO}_2$ thin film. Here, θ represents the angle between the magnetic field and the c -axis of the $\text{Nd}_{0.8}\text{Sr}_{0.2}\text{NiO}_2$. **d**, Temperature dependence of the critical magnetic field $B_c(T)$ for the magnetic fields along the c -axis (denoted as \perp), the a/b -axis ($//$, 0°), and the ab diagonal direction ($//$, 45°). Here, the B_c is defined as

the magnetic field corresponding to 50% normal resistance. The blue and the orange solid lines are the 2D G-L fittings of the $B_c(T)$ data near T_c . **e**, Polar angular dependence of the critical magnetic field $B_c(\theta)$ at $T = 6$ K. The inset shows a close-up of the $B_c(\theta)$ around $\theta = 90^\circ$. The red solid line and the blue solid line are the fittings with the 2D Tinkham model $(B_c(\theta)\sin(\theta)/B_{c//})^2 + |B_c(\theta)\cos(\theta)/B_{c\perp}| = 1$ and the 3D anisotropic mass model $B_c(\theta) = B_{c//}/(\sin^2(\theta) + \gamma^2\cos^2(\theta))^{1/2}$ with $\gamma = B_{c//}/B_{c\perp}$, respectively. **f**, **g**, Representative polar angular dependence of the magnetoresistance $R(\theta)$ at temperature $T = 5$ K under $B = 12$ T (**f**) and $B = 8$ T (**g**).

With these motivations, we investigate the polar (θ) and azimuthal (ϕ) angular dependence of the critical magnetic field and the magnetoresistance of the infinite-layer nickelate $\text{Nd}_{0.8}\text{Sr}_{0.2}\text{NiO}_2$ superconducting films. The perovskite precursor $\text{Nd}_{0.8}\text{Sr}_{0.2}\text{NiO}_3$ thin films are firstly deposited on the SrTiO_3 (001) substrates by pulsed laser deposition (PLD). The apical oxygen is then removed by the soft-chemistry topotactic reduction method using CaH_2 power. Through this procedure, the nickelate thin films undergo a topotactic transition from the perovskite phase to the infinite-layer phase, and thus the superconducting $\text{Nd}_{0.8}\text{Sr}_{0.2}\text{NiO}_2$ thin films are obtained⁵. Figure 1a presents the schematic crystal structure of $\text{Nd}_{0.8}\text{Sr}_{0.2}\text{NiO}_2$. In agreement with the previous reports⁵, the temperature-dependence of the resistance $R(T)$ exhibits metallic behavior from room temperature to low temperature followed by a superconducting transition beginning at T_c^{onset} of 14.7 K (Fig. 1b). Here, T_c^{onset} is determined at the point where $R(T)$ deviates from the extrapolation of the normal state resistance (R_N). Note that the $R(T)$ curve shows a considerably broad superconducting transition with a smooth tail, which can be described by the Berezinskii-Kosterlitz-Thouless (BKT) transition in two-dimensional (2D) superconductors²⁶⁻²⁹. As shown in the inset of Fig. 1b, the $R(T)$ curve under 0 T can be reproduced by the BKT transition using the Halperin-Nelson equation³⁰, $R = R_0 \exp \left[-2b \left(\frac{T_c' - T_{\text{BKT}}}{T - T_{\text{BKT}}} \right)^{1/2} \right]$ (R_0 and b are material-dependent parameters, and T_c' is the superconducting critical temperature), yielding

the BKT transition temperature T_{BKT} of 8.5 K. An apparent difference is also noted between the $R(T)$ curves under in-plane and out-of-plane magnetic fields (inset of Fig. 1b), implying the anisotropy of the superconductivity.

To obtain more insight into the anisotropic superconductivity in $\text{Nd}_{0.8}\text{Sr}_{0.2}\text{NiO}_2$ thin films, the critical magnetic field and magnetoresistance under different magnetic field orientations are measured. Here, the Corbino-disk configuration is used to eliminate the influence of the current flow in angular dependent magnetoresistance measurements³¹, which cannot be completely avoided in standard four-probe measurements^{32,33}. The schematic image and the optical photo of a Corbino-disk device are shown in Fig. 1c. To start with, the temperature-dependence of the critical field B_c is measured under the magnetic field applied along the c -axis (denoted as \perp), the a/b -axis (\parallel , 0°), and the ab diagonal direction (\parallel , 45°). Here, B_c is defined as the magnetic field required to reach 50% of the normal state resistance ($R_N = 98.9 \Omega$), and the $B_c(T)$ curves are collected in Fig. 1d. The T -linear dependence of $B_{c\perp}(T)$, and the $(T_c - T)^{1/2}$ -dependence of $B_{c\parallel, 0^\circ}$ and $B_{c\parallel, 45^\circ}$ near T_c show agreement with the phenomenological 2D Ginzburg-Landau (G-L) formula³⁴:

$$B_{c\perp}(T) = \frac{\phi_0}{2\pi\zeta_{\text{G-L}}^2(0)} \left(1 - \frac{T}{T_c}\right) \quad (1)$$

$$B_{c\parallel}(T) = \frac{\sqrt{12}\phi_0}{2\pi\zeta_{\text{G-L}}(0)d_{\text{sc}}} \left(1 - \frac{T}{T_c}\right)^{\frac{1}{2}} \quad (2)$$

where ϕ_0 is the flux quantum, $\zeta_{\text{G-L}}(0)$ is the zero-temperature G-L coherence length and d_{sc} is the superconducting thickness. The consistency with the 2D G-L formula near T_c indicates the 2D nature of the superconductivity in the $\text{Nd}_{0.8}\text{Sr}_{0.2}\text{NiO}_2$ thin films. To further study the dimensionality of the superconductivity, we measure the polar angular dependence of the critical magnetic field $B_c(\theta)$ for $\text{Nd}_{0.8}\text{Sr}_{0.2}\text{NiO}_2$ thin film at $T = 6$ K. Here, θ represents the angle between the magnetic field and the c -axis of the $\text{Nd}_{0.8}\text{Sr}_{0.2}\text{NiO}_2$. As shown in Fig. 1e, the $B_c(\theta)$ curve exhibits a prominent angular dependence of the external magnetic field, and a cusp-like peak is clearly resolved

around $\theta = 90^\circ$ ($B \perp c$ -axis). The peak in the $B_c(\theta)$ around 90° can be well reproduced by the 2D Tinkham model and cannot be captured by the 3D anisotropic mass model, which qualitatively demonstrates the behavior of 2D superconductivity³⁵ (inset of Fig. 1e).

To obtain a more comprehensive depiction of the anisotropy, the polar angular dependence of the magnetoresistance $R(\theta)$ at various temperatures and magnetic fields are measured, and two representative $R(\theta)$ curves at 5 K under 12 T and 8 T are shown in Figs. 1f and g, respectively. The most notable features are two sharp dips at 90° and 270° , corresponding to $B \perp c$ -axis. The two sharp dips correspond to the cusp-like peak in the $B_c(\theta)$ curve, resulting from the quasi-2D anisotropy. With varying temperatures and magnetic fields, the two sharp dips are observed in all $R(\theta)$ curves measured in the superconducting region (Supplementary Fig. 2), further confirming the quasi-2D nature of the superconducting $\text{Nd}_{0.8}\text{Sr}_{0.2}\text{NiO}_2$ thin films and suggesting that the layered superconducting NiO_2 planes should mainly account for the superconducting properties in our transport measurements. Additionally, small humps at approximately $90^\circ \pm 45^\circ$ and $270^\circ \pm 45^\circ$ are observed under 8 T and 12 T (marked by black arrows in Figs. 1f and g, respectively), while four more subtle kinks at $90^\circ \pm 20^\circ$ and $270^\circ \pm 20^\circ$ can be seen under 12 T (marked by black dashed line Fig. 1g). Considering the crystal structure of the infinite-layer nickelate, the humps and kinks with relatively small variations may originate from the magnetic moment of the rare-earth Nd^{3+} with 4f electrons, which slightly affects the superconductivity of adjacent NiO_2 planes.

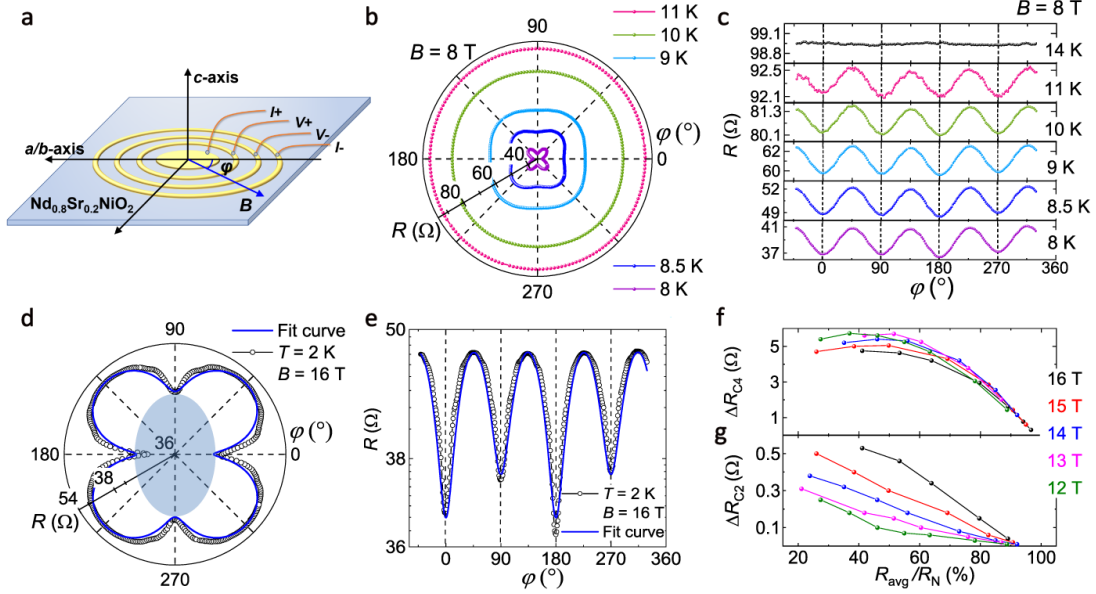


Fig. 2 | Azimuthal (ϕ) angular dependence of the magnetoresistance in $\text{Nd}_{0.8}\text{Sr}_{0.2}\text{NiO}_2$. **a**, Schematic of the Corbino-disk device for azimuthal (ϕ) angular dependent magnetoresistance measurements. Here, ϕ represents the angle between the magnetic field and the a/b -axis of the $\text{Nd}_{0.8}\text{Sr}_{0.2}\text{NiO}_2$. **b**, **c**, Azimuthal angle dependence of the magnetoresistance $R(\phi)$ at different temperatures under $B = 8$ T in the polar plot (**b**) and rectangular plot (**c**). **d**, **e**, Azimuthal angle dependence of the magnetoresistance $R(\phi)$ at $T = 2$ K under $B = 16$ T in the polar plot (**d**) and rectangular plot (**e**). Here, the logarithmic scale is used on the resistance-axis to specifically demonstrate the C_2 symmetric feature. The blue solid lines are fits with the trigonometric function: $R = R_{\text{avg}} + \Delta R_{C4} \times \sin(4\phi) + \Delta R_{C2} \times \sin(2\phi)$, where R_{avg} is the averaged magnetoresistance and ΔR_{C4} and ΔR_{C2} are the C_4 and C_2 components, respectively. The light blue area in (**d**) is a guide to the eye, representing the C_2 anisotropy. **f**, **g**, Four-fold components ΔR_{C4} (**f**) and two-fold components ΔR_{C2} (**g**) versus the ratio between the averaged magnetoresistance and the normal state resistance (R_{avg}/R_N) under different magnetic fields. Here, the values of the C_2 and C_4 components are extracted by the trigonometric function fitting.

It is noteworthy that in Fig. 1d, the $B_{c//,0^\circ}(T)$ and $B_{c//,45^\circ}(T)$ curves overlap with each other below ~ 5 T (above 9 K), but split with increasing magnetic field (decreasing

temperature), suggesting the existence of in-plane anisotropy of the superconductivity of the $\text{Nd}_{0.8}\text{Sr}_{0.2}\text{NiO}_2$ thin films. Thus, we performed the azimuthal angular dependence of the magnetoresistance $R(\varphi)$ to reveal the in-plane anisotropy of the $\text{Nd}_{0.8}\text{Sr}_{0.2}\text{NiO}_2$ thin films using the Corbino-disk configuration, as schematically shown in Fig. 2a. Here, φ represents the angle between the magnetic field and the a/b -axis of the $\text{Nd}_{0.8}\text{Sr}_{0.2}\text{NiO}_2$. The Corbino-disk configuration guarantees that the electric current flows radially from the center to the outermost electrode, which well excludes the undesired influence of the current flow and ensures that the measured anisotropy is the intrinsic properties of the $\text{Nd}_{0.8}\text{Sr}_{0.2}\text{NiO}_2$ thin films. The representative set of $R(\varphi)$ at different temperatures under 8 T in polar and rectangular plots are shown in Fig. 2b,c, respectively (more sets of $R(\varphi)$ at different temperatures and magnetic fields can be found in the Supplementary Information). Remarkably, the $R(\varphi)$ curves exhibit obvious four-fold (C_4) rotational symmetry in both polar and rectangular plots. The C_4 symmetry of the $R(\varphi)$ curves show minimum at $0^\circ, 90^\circ, 180^\circ$ and 270° (along the a/b -axis) and maximum at $45^\circ, 135^\circ, 225^\circ$ and 315° (45° to the a/b -axis) from 8 K to 11 K, and becomes indistinguishable when the temperature is increased to 14 K (the top panel in Fig. 2c).

To confirm the correspondence between the minimum of the C_4 $R(\varphi)$ and the a/b -axis of the $\text{Nd}_{0.8}\text{Sr}_{0.2}\text{NiO}_2$ thin films, control experiments have been carefully conducted. Specifically, the $\text{Nd}_{0.8}\text{Sr}_{0.2}\text{NiO}_2$ Corbino-disk device is remounted and remeasured after rotating a finite in-plane degree $\Delta\varphi$. Through the comparison between the initial results $R(\varphi)$ and the remeasured results after rotation $R(\varphi+\Delta\varphi)$, the minimum (maximum) of the C_4 symmetry are fixed with the a/b -axis (45° to the a/b -axis), verifying the C_4 symmetry of the $R(\varphi)$ is an intrinsic property of the $\text{Nd}_{0.8}\text{Sr}_{0.2}\text{NiO}_2$ thin films (Supplementary Fig. 3). Note that the $R(\varphi)$ curve at 14 K is already larger than the normal state resistance R_N of 98.9Ω , and is almost isotropic within the experimental resolution. Thus, the observed C_4 symmetry below 11 K should be related to the superconducting characteristics of the $\text{Nd}_{0.8}\text{Sr}_{0.2}\text{NiO}_2$ thin films. Moreover, considering that the quasi-2D nature of the superconductivity in the $\text{Nd}_{0.8}\text{Sr}_{0.2}\text{NiO}_2$ and the large magnetoresistance amplitudes of the C_4 anisotropy ($\Delta R_{C_4}/R$) (approximately 10% under

8 K and 8 T in Fig. 2c; around 20% under 5.5 K and 12 T in the Supplementary Fig. 6), the C_4 symmetry is not likely owing to the magnetic moment of the Nd^{3+} between the NiO_2 planes as discussed in Supplementary Fig. 8, but should be ascribed to the superconductivity in the NiO_2 planes. Previously, the C_4 symmetric $R(\varphi)$ has also been reported in the cuprates. However, the C_4 anisotropy is observed in the normal state with a magnitude of merely 0.05% and is attributed to the magnetic order³⁶, representing a different mechanism from our observations. The in-plane critical field of a d -wave superconductor is theoretically predicted to exhibit a C_4 symmetric anisotropy owing to the d -wave pairing symmetry³⁷. The C_4 anisotropic critical field as well as the C_4 anisotropic magnetoresistance have been experimentally used to determine the d -wave superconductivity in cuprate superconductors³⁸ and heavy fermion superconductors³⁹, etc. Therefore, the C_4 symmetry of our $R(\varphi)$ curves is supposed to imply the C_4 symmetric critical field of the predominant d -wave pairing in the $\text{Nd}_{0.8}\text{Sr}_{0.2}\text{NiO}_2$ thin films. The deduced d -wave pairing in the $\text{Nd}_{0.8}\text{Sr}_{0.2}\text{NiO}_2$ thin films cannot be definitely determined by our transport measurement results solely and requires further experimental investigations (e.g. phases-sensitive measurements).

Remarkably, with further increasing magnetic field, additional two-fold (C_2) symmetric signals are observed as small modulations superimposed on the primary C_4 symmetry in the $R(\varphi)$ curves. The representative $R(\varphi)$ curve under 2 K and 16 T in the polar and rectangular plots are shown in Fig. 2d and e, respectively. In addition to the predominant C_4 symmetric $R(\varphi)$, an additional C_2 signal can be clearly discerned by $R(\varphi = 0^\circ \text{ and } 180^\circ)$ being smaller than $R(\varphi = 90^\circ \text{ and } 270^\circ)$, indicating the rotational symmetry breaking between a -axis and b -axis. In the following, elaborated experiments and analysis are discussed to exclude the possible extrinsic origin of the C_2 feature. First, through the aforementioned remounted measurements after an in-plane rotation of $\Delta\varphi$, the C_2 symmetry is confirmed to be invariant with respect to the sample mounting, since $R(\varphi+\Delta\varphi)$ can nicely overlap with $R(\varphi)$ after slight shifts (Supplementary Fig. 3). Second, the C_2 features cannot be explained by the trivial misalignment of the magnetic field, because the φ angles of the C_2 symmetry maxima

are nearly corresponding to the minima of the misalignment-induced features (Supplementary Fig. 4). Third, the Corbino-disk configuration excludes the anisotropic vortex motion due to the unidirectional current flow, which has been reported in the previous works using the standard four-probe or Hall-bar electrode^{32,33}. Fourth, the C_2 features superimposed on the C_4 symmetric $R(\varphi)$ can be consistently observed in many other samples in the large magnetic field, demonstrating the strong reproducibility of the C_2 and C_4 anisotropy (Supplementary Fig. 13).

To quantitatively study the evolution of the C_2 and C_4 anisotropy of the $R(\varphi)$, the C_2 components (ΔR_{C2}) and C_4 components (ΔR_{C4}) of each $R(\varphi)$ curve at different temperatures and magnetic fields are extracted through trigonometric function fitting (Supplementary Fig. 7). Among them, the fitting curve of the $R(\varphi)$ under 2 K and 16 T is shown in Fig. 2d and e. Here, the ratio between the average resistance of the $R(\varphi)$ and the normal state resistance (R_{avg}/R_N) are used as an independent variable for an intuitive comparison. Figure 2f shows ΔR_{C4} as a function of R_{avg}/R_N under different magnetic fields, which exhibit similar parabolic behaviors with maxima approximately around 50% R_N . Differently, the ΔR_{C2} are monotonically decreasing with increasing R_{avg}/R_N as shown in Fig. 2g. With increasing magnetic field, the ΔR_{C4} show subtle decreasing tendency, while the ΔR_{C2} monotonically increase, exhibiting a magnetic field-mediated competition between the ΔR_{C4} and the ΔR_{C2} . The parabolic R_{avg}/R_N -dependence of the ΔR_{C4} can be understood as the resistance anisotropy due to the superconductivity anisotropy becomes smaller when approaching the superconducting zero-resistance state or the normal state. However, the monotonic R_{avg}/R_N -dependence of the ΔR_{C2} cannot be explained by such a scenario, suggesting a different origin of the C_2 symmetry. Generally, the observation of spontaneous rotational symmetry breaking in $R(\varphi)$ curves would indicate the existence of nematicity^{31,40}. However, in our measurements, the C_2 component has a relatively small weight in the anisotropy of the $R(\varphi)$ compared with the C_4 symmetry (<12%), inconsistent with previous results of nematic superconductivity with a primary C_2 feature³². To understand the origin of the C_2 anisotropy, we recall the RIXS-detected charge order in the nickelates that is along

the Ni-O bond direction and exhibits a competitive relationship with the superconductivity²³⁻²⁵. Considering the Ni-O bond direction of our C_2 feature and the magnetic field-mediated competition between the ΔR_{C_4} and the ΔR_{C_2} , our observation of the C_2 anisotropy might result from the charge order in $\text{Nd}_{0.8}\text{Sr}_{0.2}\text{NiO}_2$ thin films. The magnetic field suppresses the superconductivity and may alter the competition between the anisotropic superconductivity with C_4 symmetry and the charge order fluctuations with C_2 symmetry in our $\text{Nd}_{0.8}\text{Sr}_{0.2}\text{NiO}_2$, leading to the monotonically magnetic field-dependent decrease of the ΔR_{C_4} and increase of the ΔR_{C_2} in our observations (Fig. 2g). As previously reported, the Sr doping dramatically lowers the onset temperature of the charge order in the nickelates²³, which may explain the occurrence of the charge order in our $\text{Nd}_{0.8}\text{Sr}_{0.2}\text{NiO}_2$ only at low temperatures. In addition, since the C_2 feature further breaks the rotational symmetry, our observation favors a stripe-like charge order in the nickelates, which is supported by theoretical proposals^{18,19}, although further investigations are still needed.

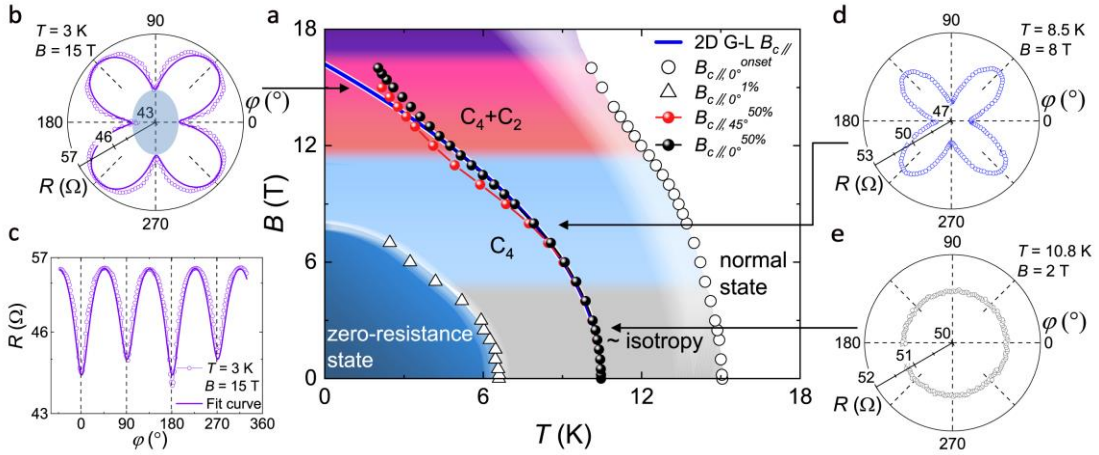


Fig. 3 | B versus T phase diagram for the $\text{Nd}_{0.8}\text{Sr}_{0.2}\text{NiO}_2$. **a**, B versus T phase diagram for in-plane magnetic fields. The white region above $B_{c//,0^\circ}^{\text{onset}}(T)$ (open circles) represents the normal state, and the dark blue region below $B_{c//,0^\circ}^{1\%}(T)$ (open triangles) denotes the zero-resistance state (defined by $R < 1\%$ of R_N). Between $B_{c//,0^\circ}^{\text{onset}}$ and $B_{c//,0^\circ}^{1\%}(T)$ is the superconducting transition region, which is separated into ~isotropy, C_4 , and C_4+C_2 regions from small magnetic field to large magnetic field regime,

depending on whether the measured $R(\varphi)$ curves exhibit nearly isotropy, C_4 or C_4+C_2 rotational symmetry. $B_{c//,0^\circ}^{50\%}(T)$ (black dots) and $B_{c//,45^\circ}^{50\%}(T)$ (red dots) represent the critical field along the a/b -axis (0°) and the ab diagonal direction (45°) determined by the 50% R_N criterion, respectively. The blue solid line is the 2D G-L fit of the $B_{c//,0^\circ}^{50\%}(T)$ data near T_c . The $B_{c//,0^\circ}^{50\%}(T)$ and $B_{c//,45^\circ}^{50\%}(T)$ data are from sample S2, which shows a more prominent upturn in the low temperature regime. **b,c,d,e**, The representative $R(\varphi)$ curves at 3 K and 15 T in the polar plot (**b**) and rectangular plot (**c**), 8.5 K and 8 T in the polar plot (**d**) and 10.8 K and 2 T in the polar plot (**e**), manifesting different rotational anisotropies. φ represents the azimuthal angle between the magnetic field and the a/b -axis of the $\text{Nd}_{0.8}\text{Sr}_{0.2}\text{NiO}_2$. The light blue area is a guide to the eye, representing the C_2 anisotropy. The black arrows approximately mark the temperature and magnetic field positions in the phase diagram where the $R(\varphi)$ curves are measured.

Based on the $B_c(T)$ curves and the anisotropic behaviors of the $R(\varphi)$, we construct the global phase diagram (Fig. 3a) to develop a comprehensive understanding of the superconductivity in the infinite-layer $\text{Nd}_{0.8}\text{Sr}_{0.2}\text{NiO}_2$ thin films. The $B_{c//,0^\circ}^{\text{onset}}(T)$ is determined at the point where the $R(T)$ curve deviates from the extrapolation of the normal state resistance under applied magnetic field. Above the $B_{c//,0^\circ}^{\text{onset}}(T)$, the $\text{Nd}_{0.8}\text{Sr}_{0.2}\text{NiO}_2$ thin films are in the normal state. The $B_{c//,0^\circ}^{1\%}(T)$ corresponds to the magnetic fields and temperatures below which the resistance R is smaller than 1% of the R_N , enclosing the region labeled as zero-resistance state in the phase diagram. The region between the $B_{c//,0^\circ}^{\text{onset}}(T)$ and the $B_{c//,0^\circ}^{1\%}(T)$ represents the superconducting transition, and is further separated into three regions labeled as \sim isotropy, C_4 and C_4+C_2 , depending on whether the corresponding $R(\varphi)$ curves exhibit nearly isotropy, C_4 , or C_4+C_2 rotational symmetry. More $R(\varphi)$ curves can be found in Supplementary Fig. 6. The representative $R(\varphi)$ curves in the polar plots are shown in

Fig.3b to e, and the arrows approximately mark the temperatures and magnetic fields where the $R(\varphi)$ curves are measured. The $B_{c//,0^\circ}^{50\%}(T)$ and $B_{c//,45^\circ}^{50\%}(T)$ curves determined by the 50% R_N criterion are also plotted in the phase diagram.

The phase diagram demonstrates an evolution of the superconducting states manifesting different rotational symmetries, depending on the external magnetic field. Specifically, in the grey region labeled as \sim isotropy ($B < 5$ T), the $B_{c//,0^\circ}^{50\%}(T)$ and $B_{c//,45^\circ}^{50\%}(T)$ curves overlap with each other and, consistently, the $R(\varphi)$ curves are nearly isotropic within our measurement resolution, indicating the isotropic superconductivity (Fig. 3e). Under the magnetic field from 5 T to 11.5 T (the blue region labeled as C_4), the $R(\varphi)$ curves exhibit C_4 rotational symmetric anisotropy (Fig. 3d), which should be ascribed to the superconductivity of the $\text{Nd}_{0.8}\text{Sr}_{0.2}\text{NiO}_2$ films since it disappears in the normal state (Fig. 2c). Simultaneously, $B_{c//,0^\circ}^{50\%}(T)$ and $B_{c//,45^\circ}^{50\%}(T)$ curves split in this region, according with the emergence of C_4 anisotropy. When the magnetic field is increased above 11.5 T (the pink region labeled as C_4+C_2), an additional C_2 anisotropy is observed in the $R(\varphi)$ curves as a superimposed modulation on the predominant C_4 anisotropy, which breaks the C_4 symmetry (Fig. 3b and c). At the same time, the $B_{c//,0^\circ}^{50\%}(T)$ curve shows an anomalous upturn at the low temperatures above 11.5 T, deviating from the saturating B_c at the low temperatures expected for a conventional superconducting state. The simultaneous occurrences of the rotational symmetry breaking in the $R(\varphi)$ curves and the enhanced superconducting critical field behavior strongly indicate the emergence of an exotic state.

The superconducting phase diagram may reveal two phase transitions characterized by spontaneous rotational symmetry breakings. The first transition occurs at approximately 5 T indicated by the change from isotropic superconductivity to C_4 anisotropy. Considering that the $R(\varphi)$ curves show the symmetry of the in-plane critical field and could reflect the superconducting pairing³⁷, the first rotational symmetry breaking may suggest a transition from s -wave to d -wave superconductivity. The

transition from s -wave to d -wave superconductivity is reminiscent of the theoretical phase diagram hosting s -, d - and $(d+is)$ -wave superconductivity for nickelates with varying parameters¹⁴. Experimentally, the s - and d -wave mixture has been reported by the previous STM study¹⁵. The second transition with the rotational symmetry turning from C_4 to C_4+C_2 takes place around 11.5 T. Also, the second transition is accompanied with an anomalous upturn of the in-plane critical field, unveiling the emergence of an electronic state unexplored before. As discussed above, we speculatively ascribe the second transition to the emergence of the charge order in the $\text{Nd}_{0.8}\text{Sr}_{0.2}\text{NiO}_2$ films. It is normally believed that the long-range charge order disfavors the superconductivity^{18,22}. In our $\text{Nd}_{0.8}\text{Sr}_{0.2}\text{NiO}_2$ films, with increasing magnetic field, the superconductivity gets suppressed and the stripe charge order fluctuation with short-range correlation emerges, accounting for the relatively small C_2 symmetric anisotropy in $R(\varphi)$ curves. The coexistence between the ordered phases with different broken symmetries is relatively rare, and the intertwined orders would give rise to more unexpected quantum phenomena and more complex phase diagram. In our $\text{Nd}_{0.8}\text{Sr}_{0.2}\text{NiO}_2$ thin films, the short-range stripe order coupled to the superconducting condensation may induce a secondary PDW state, in which the superconducting order parameter is oscillatory in space^{22,41,42}. Through pairing in the presence of the periodic potential of the charge order, the Cooper pairs gain finite center-of-mass momenta⁴², which is also a signature of the Fulde–Ferrell–Larkin–Ovchinnikov (FFLO) phase that features an upturn of the critical magnetic field at the low temperatures^{43,44}, resembling our observations. These phases were not expected previously in the $\text{Nd}_{0.8}\text{Sr}_{0.2}\text{NiO}_2$ systems. Our findings suggest that the nickelates would be a potential option to explore these exotic states.

Our experimental observations have important implications on current theoretical debates. The isotropic superconductivity requires a primary pairing mechanism that is not expected in optimally hole-doped superconducting cuprates. The successive phase transitions reveal a subtle balance between several competing interactions that are unique for infinite-layer nickelates and also cannot be explained as in cuprates. In the Mott-Kondo scenario, the phase transition may be attributed to the competition between

the Kondo coupling and the AFM spin superexchange coupling¹⁴. The Kondo coupling can produce local spin fluctuations that support isotropic s -wave pairing⁴⁵, while the AFM coupling favors d -wave pairing. In $\text{Nd}_{1-x}\text{Sr}_x\text{NiO}_2$, the superconductivity emerges around the border of the Kondo regime⁴⁶. Therefore, applying magnetic field may suppress the local spin fluctuations, tilt the balance towards AFM correlation, and thus induce a secondary d -wave component, which explains the emergent C_4 symmetry by either d - or $(d+is)$ -wave pairing¹⁴. The charge order also competes with the AFM correlation¹⁹ as well as the superconductivity. Previous experiments have shown that the charge order phase boundary may even penetrate into the superconducting dome. Further increasing magnetic field may reduce both the superconductivity and AFM correlation, thus promote the charge order, and lead to the observed C_2 symmetry. The interplay of the Kondo effect, the AFM correlation, the superconductivity, and the charge order provides a potential playground for novel correlated phenomena, which is well beyond a simple scenario. Any candidate theory should be made in conformity with all these experimental observations.

In summary, we systematically investigated the angular dependence of the transport properties of the infinite-layer nickelate $\text{Nd}_{0.8}\text{Sr}_{0.2}\text{NiO}_2$ thin films with Corbino-disk configuration. The evident polar angular dependent anisotropy strongly indicates the quasi-2D nature of the superconductivity in $\text{Nd}_{0.8}\text{Sr}_{0.2}\text{NiO}_2$ thin films. The azimuthal angular dependence of the magnetoresistance $R(\varphi)$ curves manifest different rotational symmetric structures depending on the external magnetic fields, which are summarized in the B versus T phase diagram. With increasing magnetic field, the $R(\varphi)$ curves exhibit isotropic, C_4 symmetric, and then C_4+C_2 symmetric behaviors successively, demonstrating the emergence of the quantum states characterized by spontaneous rotational symmetry breaking. Since the symmetry of the $R(\varphi)$ curves could reflect the symmetry of the superconducting order parameter, the observed $R(\varphi)$ curves evolving from isotropy to C_4 anisotropy may suggest an extraordinary superconducting pairing of the $\text{Nd}_{0.8}\text{Sr}_{0.2}\text{NiO}_2$ beyond the familiar cuprate scenario. In the low temperature and large magnetic field regime, we find a striking concurrence of

an additional C_2 symmetric modulations in the $R(\varphi)$ curves and an anomalous upturn of the temperature-dependent critical magnetic field. We speculate that the C_2 feature in the $R(\varphi)$ curves may result from the stripe charge order fluctuations in the $\text{Nd}_{0.8}\text{Sr}_{0.2}\text{NiO}_2$, which can coexist with the superconductivity, and might potentially give rise to a charge order-driven PDW state. Our findings shed new light on the dimensionality and the pairing symmetry of the superconductivity in the infinite-layer nickelate $\text{Nd}_{0.8}\text{Sr}_{0.2}\text{NiO}_2$ thin films, and reveal that the superconducting $\text{Nd}_{0.8}\text{Sr}_{0.2}\text{NiO}_2$ is a promising material platform to study the unconventional superconductivity and the interplay between the various exotic states.

References

1. Bardeen, J., Cooper, L. N., Schrieffer, J. R. Microscopic Theory of Superconductivity. *Phys. Rev.* **106**, 162-164 (1957).
2. Mcmillan, W. L. Transition Temperature of Strong-Coupled Superconductors. *Phys. Rev.* **167**, 331-344 (1968).
3. Wollman, D. A., Van Harlingen, D. J., Lee, W. C., Ginsberg, D. M., Leggett, A. J. Experimental determination of the superconducting pairing state in YBCO from the phase coherence of YBCO-Pb dc SQUIDs. *Phys. Rev. Lett.* **71**, 2134-2137 (1993).
4. Tsuei, C. C., Kirtley, J. R. Pairing symmetry in cuprate superconductors. *Rev. Mod. Phys.* **72**, 969-1016 (2000).
5. Li, D. et al. Superconductivity in an infinite-layer nickelate. *Nature* **572**, 624-627 (2019).
6. Pickett, W. E. The dawn of the nickel age of superconductivity. *Nat. Rev. Phys.* **3**, 7-8 (2020).
7. Norman, M. R. Entering the Nickel Age of Superconductivity. *Physics* **13**, 85 (2020).
8. Gu, Q., Wen, H. H. Superconductivity in nickel-based 112 systems. *The Innovation* **3**, 100202 (2022).
9. Nomura, Y., Arita, R. Superconductivity in infinite-layer nickelates. *Rep. Prog. Phys.* **85**, 052501 (2022).
10. Sakakibara, H. et al. Model Construction and a Possibility of Cupratelike Pairing in a New d^9 Nickelate Superconductor $(\text{Nd, Sr})\text{NiO}_2$. *Phys. Rev. Lett.* **125**, 077003 (2020).
11. Wu, X. et al. Robust $d_{x^2-y^2}$ -wave superconductivity of infinite-layer nickelates. *Phys. Rev. B* **101**,

- 060504 (2020).
12. Adhikary, P., Bandyopadhyay, S., Das, T., Dasgupta, I., Saha-Dasgupta, T. Orbital-selective superconductivity in a two-band model of infinite-layer nickelates. *Phys. Rev. B* **102**, 100501(R) (2020).
 13. Bandyopadhyay, S., Adhikary, P., Das, T., Dasgupta, I., Saha-Dasgupta, T. Superconductivity in infinite-layer nickelates: Role of f orbitals. *Phys. Rev. B* **102**, 220502(R) (2020).
 14. Wang, Z., Zhang, G.-M., Yang, Y.-f., Zhang, F.-C. Distinct pairing symmetries of superconductivity in infinite-layer nickelates. *Phys. Rev. B* **102**, 220501(R) (2020).
 15. Gu, Q. et al. Single particle tunneling spectrum of superconducting $\text{Nd}_{1-x}\text{Sr}_x\text{NiO}_2$ thin films. *Nat. Commun.* **11**, 6027 (2020).
 16. Chow, L. E. et al. Pairing symmetry in infinite-layer nickelate superconductor. Preprint at <http://arxiv.org/abs/2207.00266> (2022).
 17. Harvey, S. P. et al. Evidence for nodal superconductivity in infinite-layer nickelates. Preprint at <http://arxiv.org/abs/2201.12971> (2022).
 18. Shen, Y., Qin, M., Zhang, G.-M. Comparative study of the charge order in the undoped infinite-layer nickelate superconductors. Preprint at <http://arxiv.org/abs/2207.00266> (2022).
 19. Chen, H., Yang, Y.-f., Zhang, G.-M. Charge order from the local Coulomb repulsion in undoped infinite-layer nickelates. Preprint at <http://arxiv.org/abs/2204.12208> (2022).
 20. Lu, H. et al. Magnetic excitations in infinite-layer nickelates. *Science* **373**, 213-216 (2021).
 21. Dagotto, E. Complexity in Strongly Correlated Electronic Systems. *Science* **309**, 257-262 (2005).
 22. Fradkin, E., Kivelson, S. A., Tranquada, J. M. Theory of intertwined orders in high temperature superconductors. *Rev. Mod. Phys.* **87**, 457-482 (2015).
 23. Rossi, M. et al. A broken translational symmetry state in an infinite-layer nickelate. *Nat. Phys.* **18**, 869-873 (2022).
 24. Tam, C. C. et al. Charge density waves in infinite-layer NdNiO_2 nickelates. *Nat. Mater.* **21**, 1116–1120 (2022).
 25. Krieger, G. et al. Charge and Spin Order Dichotomy in NdNiO_2 Driven by the Capping Layer. *Phys. Rev. Lett.* **129**, 027002 (2022).
 26. Berezinskii, V. L. Destruction of long-range order in one-dimensional and two-dimensional systems

- having a continuous symmetry group. I. Classical systems. *Sov. Phys.—JETP* **32**, 493 (1971).
27. Kosterlitz, J. M., Thouless, D. J. Ordering, metastability and phase transitions in two-dimensional systems. *J. Phys. C: Solid State Phys.* **6**, 1181-1203 (1973).
 28. Reyren, N. et al. Superconducting Interfaces Between Insulating Oxides. *Science* **317**, 1196-1199 (2007).
 29. Zhang, W.-H. et al. Direct Observation of High-Temperature Superconductivity in One-Unit-Cell FeSe Films. *Chin. Phys. Lett.* **31**, 017401 (2014).
 30. Halperin, B. I., Nelson, D. R. Resistive transition in superconducting films. *J. Low Temp. Phys.* **36**, 599-616 (1979).
 31. Xiang, Y. et al. Twofold symmetry of *c*-axis resistivity in topological kagome superconductor CsV₃Sb₅ with in-plane rotating magnetic field. *Nat. Commun.* **12**, 6727 (2021).
 32. Iye, Y. et al. Dissipation in the mixed state of conventional and high temperature superconductors. *Phys. C Supercond.* **167**, 278-286 (1990).
 33. Wang, B. Y. et al. Rare-Earth Control of the Superconducting Upper Critical Field in InfiniteLayer Nickelates. Preprint at <http://arxiv.org/abs/2205.15355> (2022).
 34. Harper, F. E., Tinkham, M. The Mixed State in Superconducting Thin Films. *Phys. Rev.* **172**, 441-450 (1968).
 35. Tinkham, M. *Introduction to superconductivity*, (Courier Corporation, 2004).
 36. Jovanović, V. P., Fruchter, L., Li, Z. Z., Raffy, H. Anisotropy of the in-plane angular magnetoresistance of electron-doped Sr_{1-x}La_xCuO₂ thin films. *Phys. Rev. B* **81**, 134520 (2010).
 37. Takanaka, K., Kuboya, K. Anisotropy of upper critical field and pairing symmetry. *Phys. Rev. Lett.* **75**, 323-325 (1995).
 38. Koike, Y., Takabayashi, T., Noji, T., Nishizaki, T., Kobayashi, N. Fourfold symmetry in the ab plane of the upper critical field for single-crystal Pb₂Sr₂Y_{0.62}Ca_{0.38}Cu₃O₈: Evidence for *d*_{x²-y²} pairing in a high-Tc superconductor. *Phys. Rev. B* **54**, R776-R779 (1996).
 39. Vieyra, H. A. et al. Determination of gap symmetry from angle-dependent *Hc*₂ measurements on CeCu₂Si₂. *Phys. Rev. Lett.* **106**, 207001 (2011).
 40. Fradkin, E., Kivelson, S. A., Lawler, M. J., Eisenstein, J. P., Mackenzie, A. P. Nematic Fermi Fluids in Condensed Matter Physics. *Annu. Rev. Condens. Matter Phys.* **1**, 153-178 (2010).

41. Berg, E., Fradkin, E., Kivelson, S. A. Theory of the striped superconductor. *Phys. Rev. B* **79**, 064515 (2009).
42. Liu, X., Chong, Y. X., Sharma, R., Davis, J. C. S. Discovery of a Cooper-pair density wave state in a transition-metal dichalcogenide. *Science* **372**, 1447-1452 (2021).
43. Fulde, P., Ferrell, R. A. Superconductivity in a Strong Spin-Exchange Field. *Phys. Rev.* **135**, A550-A563 (1964).
44. Larkin, A. I., Ovchinnikov, Y. N. Inhomogeneous state of superconductors. *Zh. Eksp. Teor. Fis.* **47**, 1136(1964). *Sov. Phys. JETP* **20**, 762 (1965).
45. Bodensiek, O., Žitko, R., Vojta, M., Jarrell, M., Pruschke, T. Unconventional Superconductivity from Local Spin Fluctuations in the Kondo Lattice. *Phys. Rev. Lett.* **110**, 146406 (2013).
46. Shao, T. N. et al. Kondo scattering in underdoped $\text{Nd}_{1-x}\text{Sr}_x\text{NiO}_2$ infinite-layer superconducting thin films. Preprint at <http://arxiv.org/abs/2209.06400> (2022).

Method.

Thin-film synthesis.

The samples were grown on SrTiO₃ substrates using pulsed laser deposition under growth and reduction conditions previously reported⁴⁷. The Nd_{0.8}Sr_{0.2}NiO₂ films with infinite-layer structure are prepared by topochemical reduction of perovskite Nd_{0.8}Sr_{0.2}NiO₃ films (thickness about 14.5~16 nm) without capping layer. The precursor Nd_{0.8}Sr_{0.2}NiO₃ films are deposited on the TiO₂-terminated SrTiO₃ (001) substrates by 248 nm KrF laser. The substrate temperature is controlled at 620 °C with an oxygen pressure of 200 mTorr during the deposition. A laser fluence of 1 J/cm² was used to ablate the target and the size of laser spot is about 3 mm². After deposition, the samples were cooled down in the same oxygen pressure at the rate of 10 °C/min. To obtain the infinite-layer phase, the samples were sealed in the quartz tube together with 0.1g CaH₂. The pressure of the tube is about 0.3 mTorr. Then, the tube was heated up to 300 °C in tube furnace, hold for 2 hours, and naturally cooled down with the ramp rate of 10 °C/min.

Devices fabrication.

The Corbino-disk electrode is fabricated using the standard photolithography technique. After spin coating of PMMA on the Nd_{0.8}Sr_{0.2}NiO₂ thin film samples, the annular electrodes were patterned through electron beam lithography in a FEI Helios NanoLab 600i Dual Beam System. Then, the metal electrodes (Ti/Au, 6.5/100 nm) were deposited in a LJUHVE-400 L E-Beam Evaporator. After that, the PMMA layers were removed by the standard lift-off process. Finally, the electrodes are contacted using wire-bonded Al wires for transport measurements.

Transport measurements.

The angle-dependent transport measurements were carried out on a rotator with an accuracy of 0.01° in a 16 T-Physical Property Measurement System (PPMS-EverCool-16, Quantum Design).

Data availability

Source data are provided with this paper. All other data that support the plots within this paper and other findings of this study are available from the corresponding author upon reasonable request.

References

47. Ding, X. et al. Stability of superconducting $\text{Nd}_{0.8}\text{Sr}_{0.2}\text{NiO}_2$ thin films. *Sci. China-Phys. Mech. Astron.* **65**, 267411 (2022).

Acknowledgements

We acknowledge insightful discussions with Yanzhao Liu, Ying Xing, Qizhi Li, Yingying Peng, and Huiqian Luo. This work was financially supported by Beijing Natural Science Foundation (Z180010), the National Natural Science Foundation of China (Grant No. 11888101), the National Key Research and Development Program of China (Grant No. 2018YFA0305604), the National Natural Science Foundation of China (No. 12174442), the Strategic Priority Research Program of Chinese Academy of Sciences (Grant No. XDB28000000), the Fundamental Research Funds for the Central Universities and the Research Funds of Renmin University of China. L.Q. and X.D. were supported by the National Natural Science Foundation of China (Grant Nos. 12274061, 52072059, and 11774044). Y.F.Y. was supported by the National Natural Science Foundation of China (NSFC Grants No. 11974397), and the Strategic Priority Research Program of the Chinese Academy of Sciences (Grant No. XDB33010100).

Author contributions

J.W. conceived and instructed the research. H.R.J., Y.N.L., Y.L., Z.Y.X. and S.C.Q. fabricated the Corbino-disk devices, performed the transport measurements and analyzed the data under the guidance of J.W.. X.D. and L.Q. synthesized the thin film samples. Y.F.Y. and G.M.Z. contributed to the theoretical explanations. H.R.J., Y.N.L.

Y.L. and J.W. wrote the manuscript with input from all authors.

Competing interests

The authors declare no competing interests.

Supplementary Information for
“Rotational symmetry breaking in superconducting nickelate $\text{Nd}_{0.8}\text{Sr}_{0.2}\text{NiO}_2$
films”

Haoran Ji^{1#}, Yanan Li^{1#}, Yi Liu^{2#}, Xiang Ding^{3#}, Zheyuan Xie¹, Shichao Qi¹, Liang Qiao^{3*}, Yi-feng Yang^{4,5,6}, Guang-Ming Zhang^{7,8} and Jian Wang^{1,9,10,11*}

¹International Center for Quantum Materials, School of Physics, Peking University, Beijing 100871, China

²Department of Physics, Renmin University of China, Beijing 100872, China

³School of Physics, University of Electronic Science and Technology of China, Chengdu 610054, China

⁴Beijing National Lab for Condensed Matter Physics and Institute of Physics, Chinese Academy of Sciences, Beijing 100190, China

⁵School of Physical Sciences, University of Chinese Academy of Sciences, Beijing 100049, China

⁶Songshan Lake Materials Laboratory, Dongguan, Guangdong 523808, China

⁷State Key Laboratory of Low-Dimensional Quantum Physics and Department of Physics, Tsinghua University, Beijing 100084, China.

⁸Frontier Science Center for Quantum Information, Beijing 100084, China

⁹Collaborative Innovation Center of Quantum Matter, Beijing 100871, China

¹⁰CAS Center for Excellence in Topological Quantum Computation, University of Chinese Academy of Sciences, Beijing 100190, China

¹¹Beijing Academy of Quantum Information Sciences, Beijing 100193, China

#These authors contribute equally: Haoran Ji, Yanan Li, Yi Liu and Xiang Ding.

*Corresponding author. jianwangphysics@pku.edu.cn (J.W.), liang.qiao@uestc.edu.cn (L.Q.).

I. Additional information for sample S1

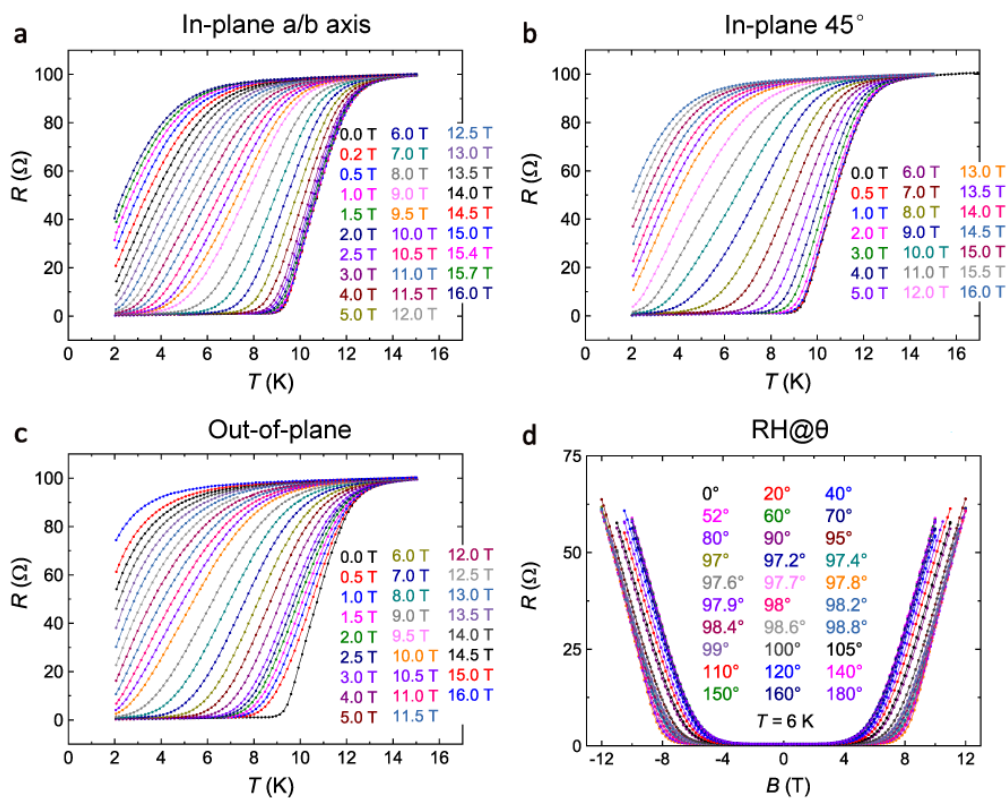


Fig. S1. $R(T)$ and $R(H)$ curves for the determination of B_c . $R(T)$ under different magnetic field applied along the a/b -axis (**a**), the ab diagonal direction (**b**), and the c -axis (**c**), **d**, $R(B)$ at different θ angles at 6 K. The $B_{c//, 0^\circ}(T)$, $B_{c//, 45^\circ}(T)$, $B_{c\perp}(T)$ and $B_c(\theta)$ are determined using the 50% R_N criterion through the data shown in **a**, **b**, **c** and **d**, respectively.

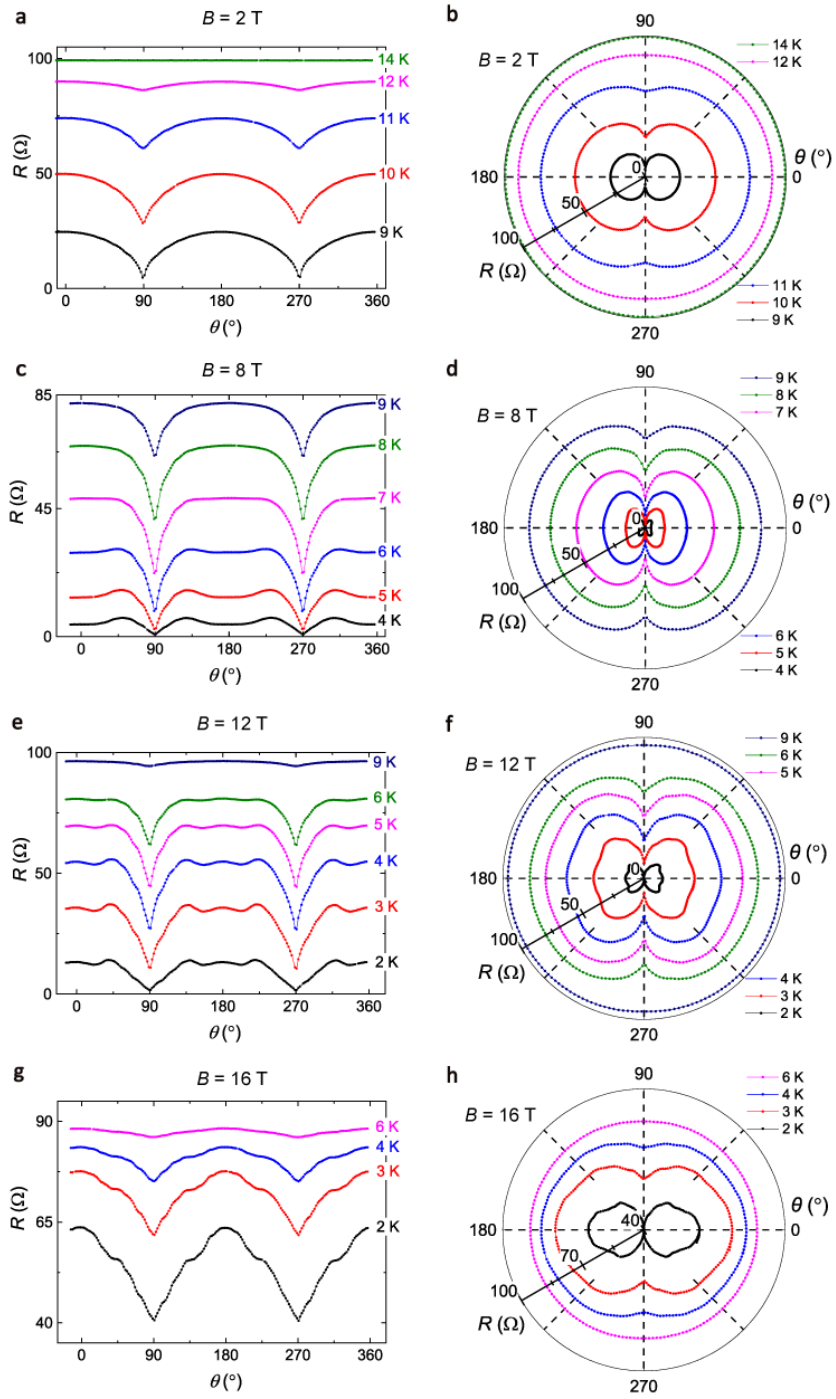


Fig. S2. $R(\theta)$ curves showing the quasi-2D anisotropy. Polar angular dependence of magnetoresistance $R(\theta)$ at different temperatures under 2 T (**a** and **b**), 8 T (**c** and **d**), 12 T (**e** and **f**) and 16 T (**g** and **h**). Here, θ represents the angle between the magnetic field and the c -axis of the $\text{Nd}_{0.8}\text{Sr}_{0.2}\text{NiO}_2$. The left panels show the rectangular plots and the right panels show the corresponding polar plots.

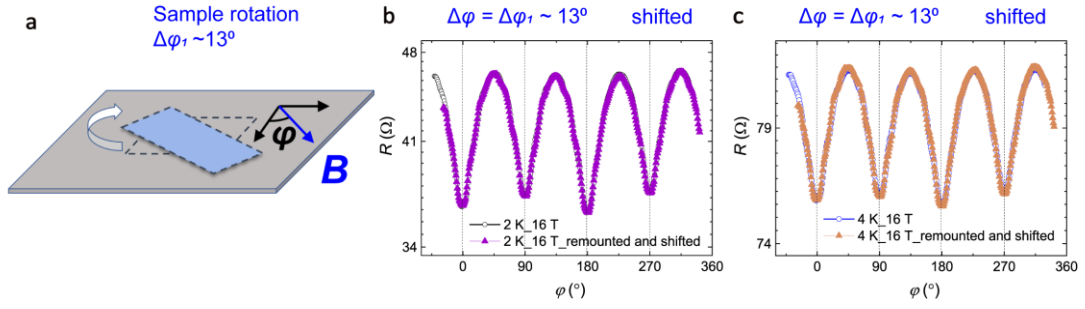


Fig. S3. Remounted measurements after an in-plane rotation $\Delta\phi_2$. **a**, Schematic of the sample remounting after an in-plane rotation. **b**, **c**, The comparison between the initial results $R(\phi)$ and the remeasured results $R(\phi+\Delta\phi_1)$ after an in-plane rotation $\Delta\phi_1 \sim 13^\circ$. The $R(\phi)$ and $R(\phi+\Delta\phi_1)$ curves under 16 T at 2 K (**b**) and 3 K (**c**) show the C_4+C_2 anisotropy. The $R(\phi+\Delta\phi_1)$ curves are shifted 13° and 1.6Ω for comparison, which can nicely overlap with initial $R(\phi)$ curves, confirming that the C_4+C_2 anisotropy is intrinsic.

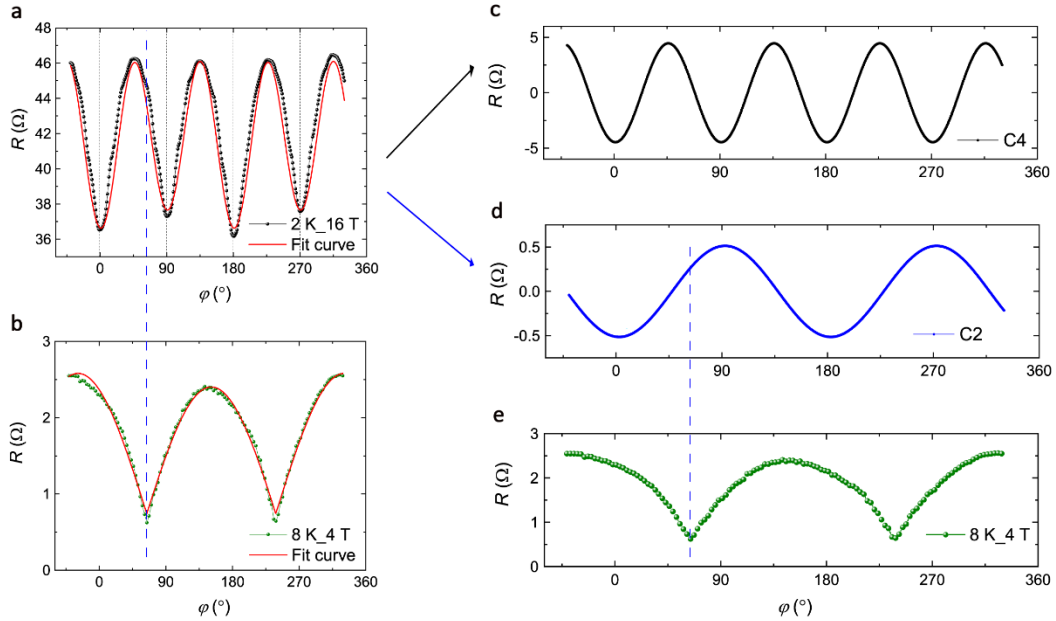


Fig. S4. Exclusion of the possibility that the C_2 features are due to the misalignment. **a**, $R(\phi)$ under 16 T at 2 K, and the fit with the trigonometric function $R = R_{\text{avg}} + \Delta R_{C_4} \times \sin(4\phi) + \Delta R_{C_2} \times \sin(2\phi)$, where R_{avg} is the averaged magnetoresistance and ΔR_{C_4} and ΔR_{C_2} are the C_4 and C_2 components, respectively (red solid line). **b** and **e**, $R(\phi)$ under 8 T at 2 K showing the misalignment-induced two-sharp-dips feature, and

the fit with $R = R_{\text{avg}} + \Delta R_{\text{misalignment}} \times |\sin(2\varphi) - s_1|$, where $\Delta R_{\text{misalignment}}$ is the misalignment component and s_1 is a fitting parameter (red solid line)⁴⁸. The C_4 component (**c**) and C_2 component (**d**) are extracted by the trigonometric function fitting in **a**. The angle positions of the maximum of the C_2 symmetry (**d**) roughly correspond to the minimum of the misalignment-induced feature (**e**), as indicated by the blue dashed line, confirming that the C_2 anisotropic feature is not due to the trivial misalignment between the sample plane and the magnetic field. In the large magnetic field regime, the polar angular dependent anisotropy is weak, because the anisotropy ratio of the in-plane critical field to the out-of-plane critical field ($\Gamma = B_{c\parallel}/B_{c\perp}$) becomes smaller with increasing field, and is gradually approaching 1 (see Fig. 1d in the main text). Thus, the influence of the misaligned magnetic field is negligible in large magnetic field regime.

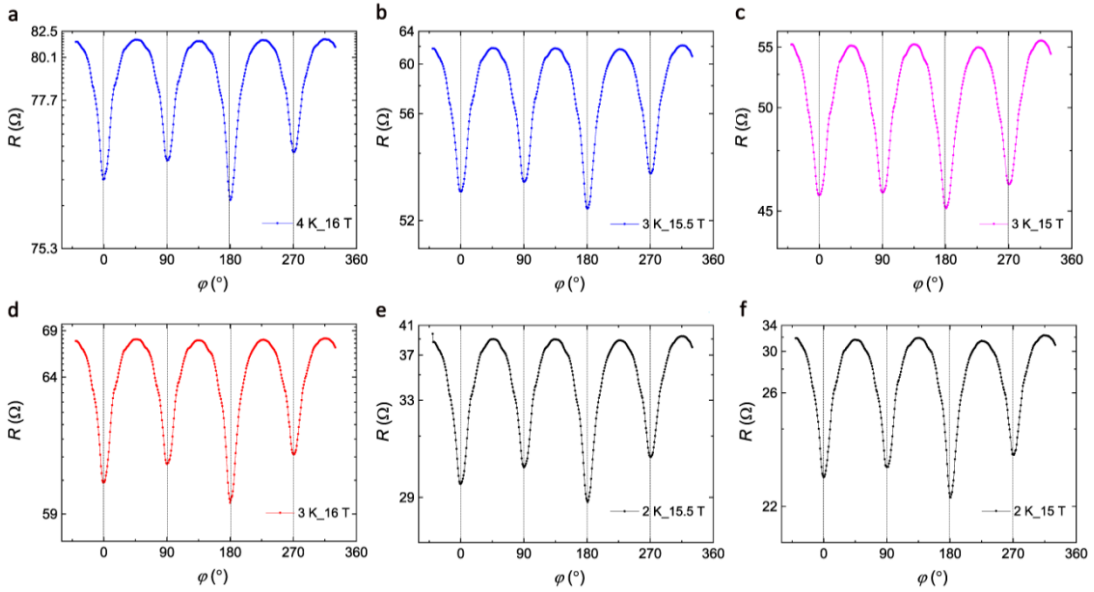


Fig. S5. Reproducible C_4+C_2 anisotropy at different temperatures and magnetic fields. Azimuthal angular dependence of magnetoresistance $R(\varphi)$ curves showing reproducible C_4+C_2 symmetry at 4 K and 16 T (**a**), 3 K and 16 T (**d**), 3 K and 15.5 T (**b**), 2 K and 15.5 T (**e**), 3 K and 15 T (**c**) and 2 K and 15 T (**f**). The logarithmic scale is used on the resistance axis.

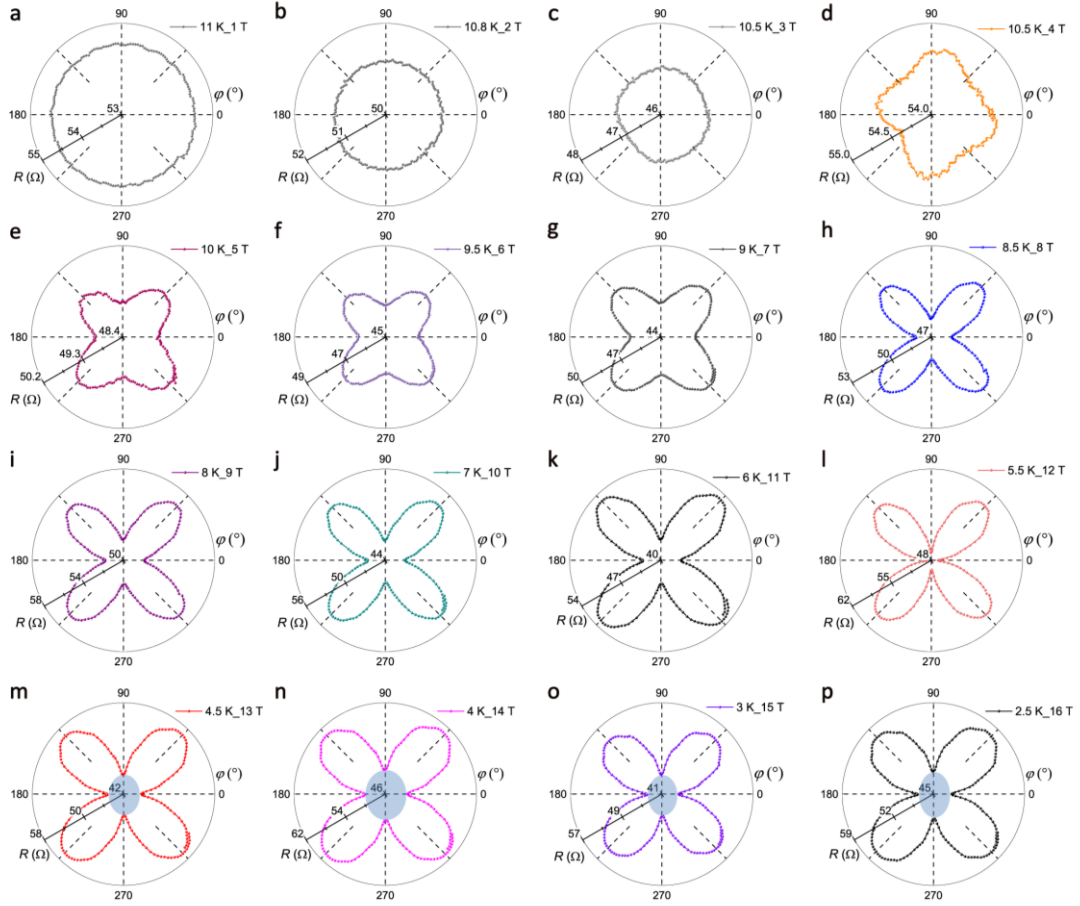


Fig. S6. $R(\varphi)$ curves at different temperatures and magnetic fields. $R(\varphi)$ curves in the polar plots at different temperatures and magnetic fields from 1 T to 16 T (a to p), showing the evolution of the rotational symmetry from isotropic to C_4 symmetric and then to C_4+C_2 anisotropic. The temperatures and magnetic fields are labeled in the corresponding plots. The blue areas are guides to the eye, representing the C_2 anisotropy.

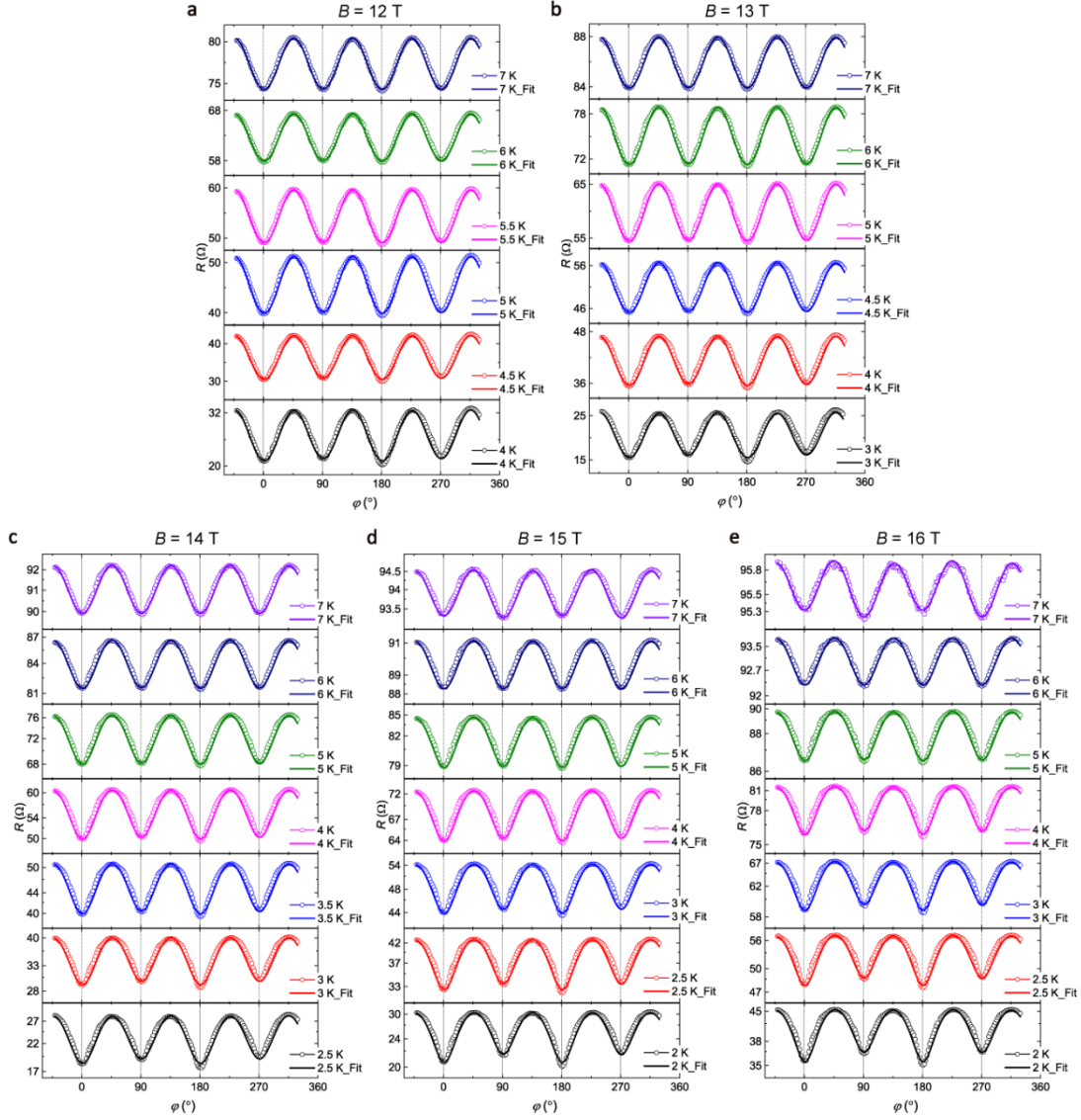


Fig. S7. Fit of the C_4+C_2 symmetric $R(\varphi)$ curves at different temperatures and magnetic fields. $R(\varphi)$ curves and the corresponding trigonometric function fits at different temperatures and magnetic fields from 12 T to 16 T (a to e). Each $R(\varphi)$ curve is fitted by the trigonometric function $R = R_{\text{avg}} + \Delta R_{C_4} \times \sin(4\varphi) + \Delta R_{C_2} \times \sin(2\varphi)$ to extract the C_2 component (ΔR_{C_2}) and C_4 component (ΔR_{C_4}). Here, the logarithmic scale is used on the resistance-axis in (c to e) to specifically demonstrate the C_2 symmetric feature.

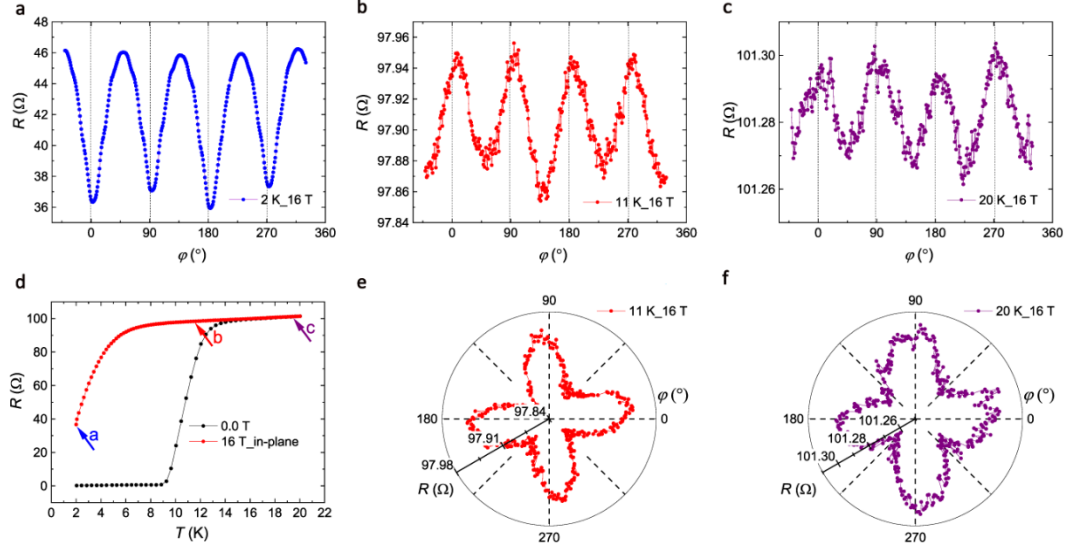


Fig. S8. C_4 anisotropy in the $R(\varphi)$ curves of the superconducting state and the normal state. **a**, Rectangular plot of the $R(\varphi)$ curve measured at 2 K and 16 T where the $\text{Nd}_{0.8}\text{Sr}_{0.2}\text{NiO}_2$ is in the superconducting transition, showing C_4+C_2 anisotropy. **b** and **e**, Rectangular plot (**b**) and polar plot (**e**) of the $R(\varphi)$ curves measured at 11 K and 16 T where the $\text{Nd}_{0.8}\text{Sr}_{0.2}\text{NiO}_2$ is in the normal state, showing C_4 and C_2 anisotropy with different orientations and two orders of magnitude smaller compared with (**a**). **c** and **f**, Rectangular plot (**c**) and polar plot (**f**) of the $R(\varphi)$ curves measured at 20 K and 16 T where the $\text{Nd}_{0.8}\text{Sr}_{0.2}\text{NiO}_2$ is in the normal state, showing C_4 anisotropy. **d**, $R(T)$ curves under 0 T and 16 T. Three arrows indicate the corresponding temperature where (**a**), (**b**) and (**c**) are measured. The $R(\varphi)$ curves shown here are measured with a current of $5 \mu\text{A}$. The C_4 symmetry with a smaller magnitude observed in the normal state of the $\text{Nd}_{0.8}\text{Sr}_{0.2}\text{NiO}_2$ can be ascribed to the magnetic moment of the rare-earth Nd^{3+} . The magnetic order-induced C_4 symmetric $R(\varphi)$ curves have also been reported in the cuprates previously³⁶, which is observed in the normal state³⁶ with a magnitude of 0.05%, consistent with our Nd^{3+} -resultant C_4 anisotropy in the normal state. However, such a phenomenon cannot explain the C_4 anisotropy measured in the superconducting transition region, which shows different orientations (C_4 exhibits minima at 0° , 90° , 180° and 270° in the superconducting region, instead of 45° , 135° , 225° and 315° in the normal state) and much stronger magnitude (two orders of magnitude larger).

Furthermore, the anisotropy in the normal state is absent below 16 T. For example, the $R(\varphi)$ curve of the normal state is isotropic under 8 T as shown in Fig. 2c in the main text. Differently, the anisotropy in the superconducting transition region emerges approximately above 5 T.

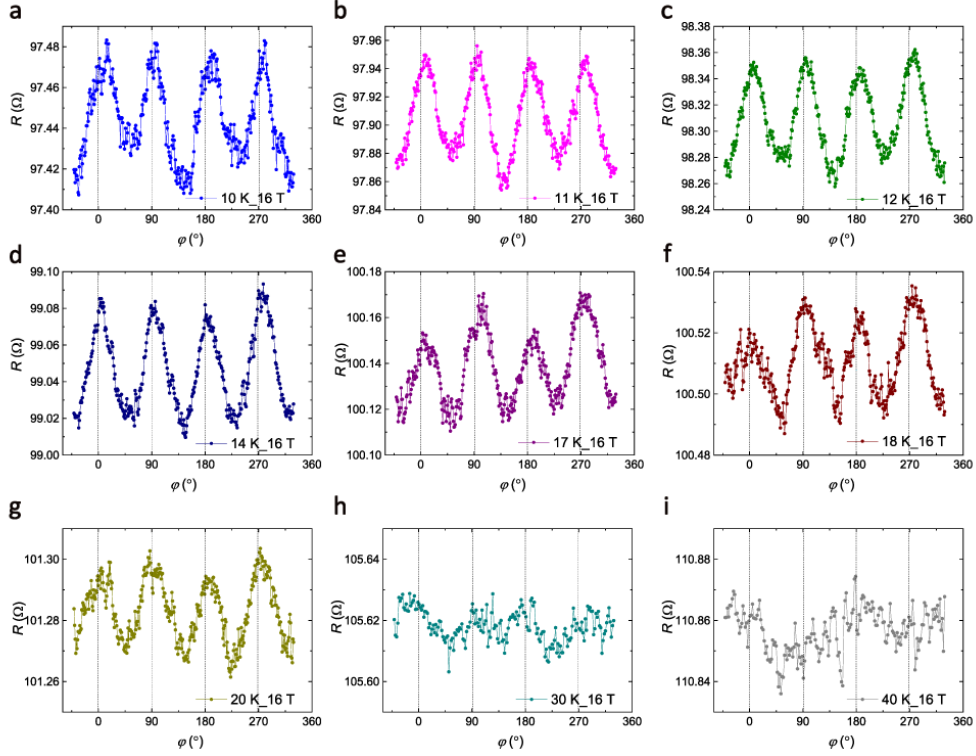


Fig. S9. C_4 anisotropy in the $R(\varphi)$ curves of the normal state. $R(\varphi)$ curves under 16 T at different temperatures in the rectangular plots (a to i), where the $\text{Nd}_{0.8}\text{Sr}_{0.2}\text{NiO}_2$ thin film is in the normal state. The temperatures and magnetic fields are labeled in the corresponding plots. The C_4 anisotropy smears out with increasing temperature, and is indistinguishable above 30 K. The measured current is 5 μA . The anisotropy in the normal state is absent below 16 T. For example, the $R(\varphi)$ curve of the normal state is isotropic under 8 T as shown in Fig. 2c in the main text. Differently, the anisotropy in the superconducting transition region emerges approximately above 5 T.

II. Reproducible results in sample S2

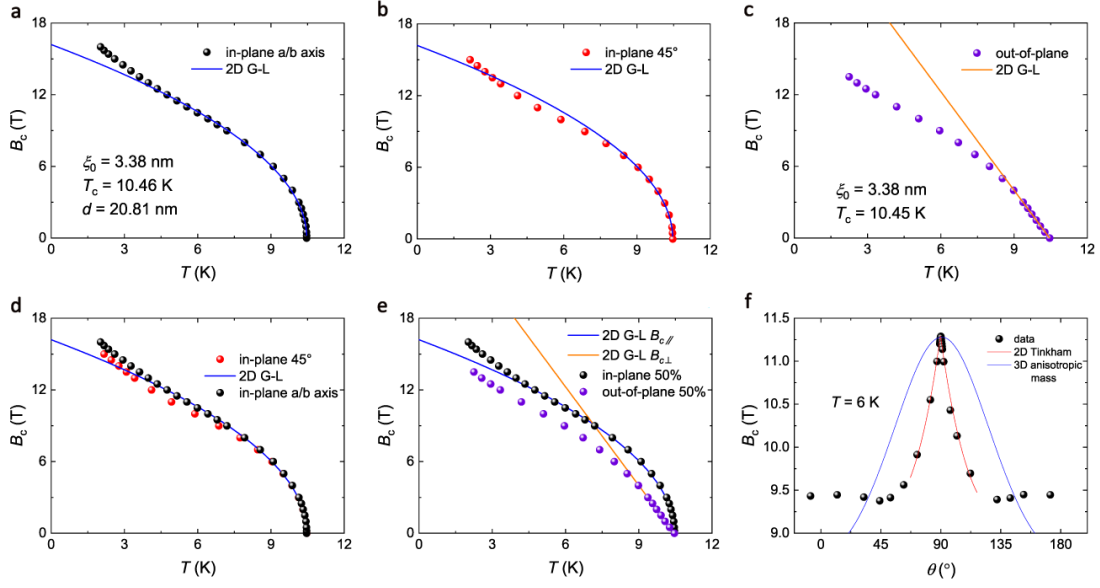


Fig. S10. Reproducible critical field behaviors in sample S2. Temperature dependence of the critical magnetic field measured along a/b -axis **(a)**, the ab diagonal direction **(b)**, and c -axis **(c)**, **d**, Comparison between the $B_{c//,0^\circ}^{50\%}(T)$ and $B_{c//,45^\circ}^{50\%}(T)$. **e**, Comparison between $B_{c//,0^\circ}^{50\%}(T)$ and $B_{c\perp}^{50\%}(T)$. The blue and the orange solid lines are the 2D G-L fittings of the $B_c(T)$ data near T_c . **f**, B_c at different θ angles at 6 K. The red solid line and blue solid line represent the theoretical fitting curves obtained by 2D Tinkham model and 3D anisotropic mass model, respectively.

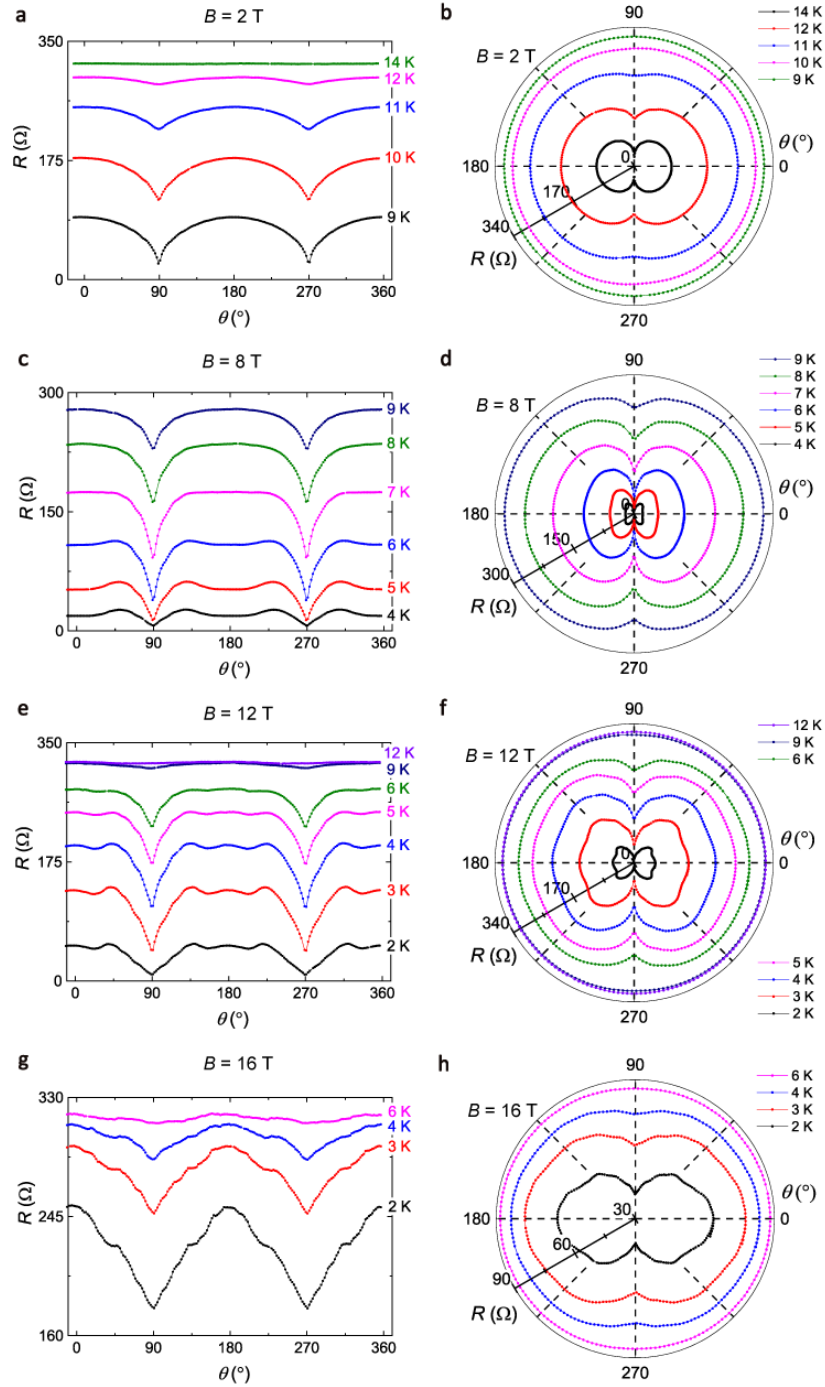


Fig. S11. Reproducible quasi-2D anisotropy in sample S2. Polar angular dependence of magnetoresistance $R(\theta)$ for sample S2 at different temperatures under 2 T (**a** and **b**), 8 T (**c** and **d**), 12 T (**e** and **f**), and 16 T (**g** and **h**). The left panels show the rectangular plots and the right panels show the corresponding polar plots.

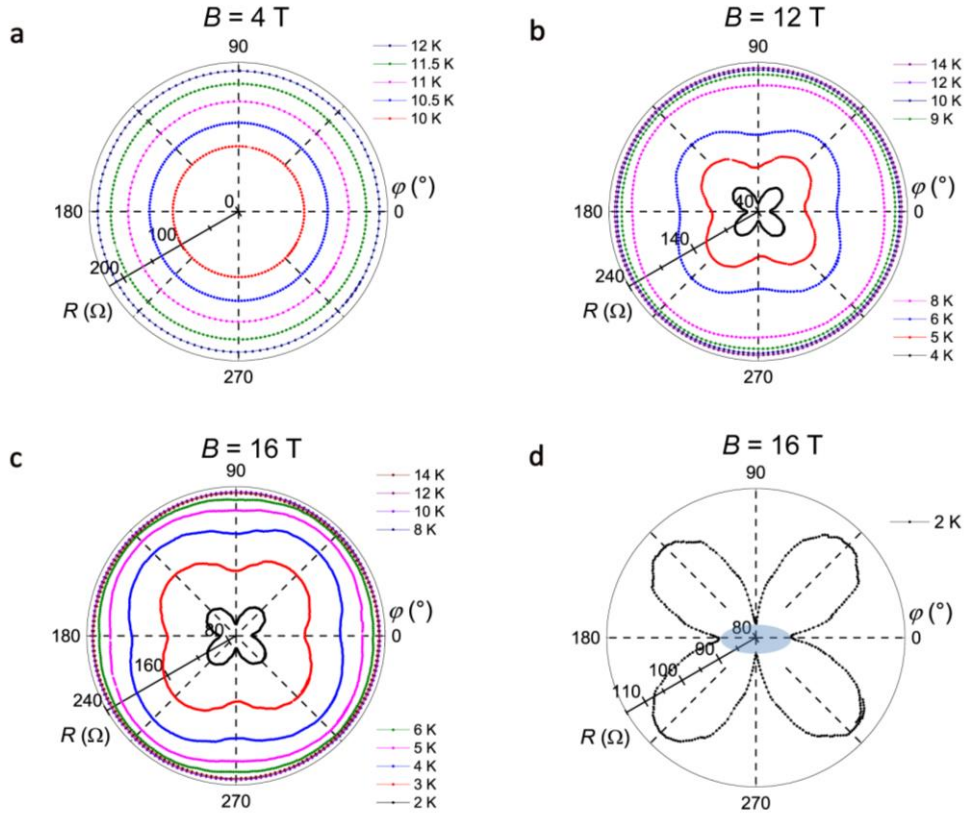


Fig. S12. Reproducible $R(\varphi)$ behaviors in sample S2. Azimuthal angular dependence of magnetoresistance $R(\varphi)$ for sample S2 at different temperatures under 4 T (a), 12 T (b), 16 T (c) in the polar plots, showing nearly isotropy, C_4 anisotropy, and C_4+C_2 anisotropy, respectively. The $R(\varphi)$ curve at 2 K and 16 T is further plotted in (d), where the C_2 anisotropy can be better resolved. The blue area is a guide to the eye, representing the C_2 anisotropy.

III. Reproducible C_2 symmetry superimposed on the C_4 symmetry in other three samples (S2, S3 and S4).

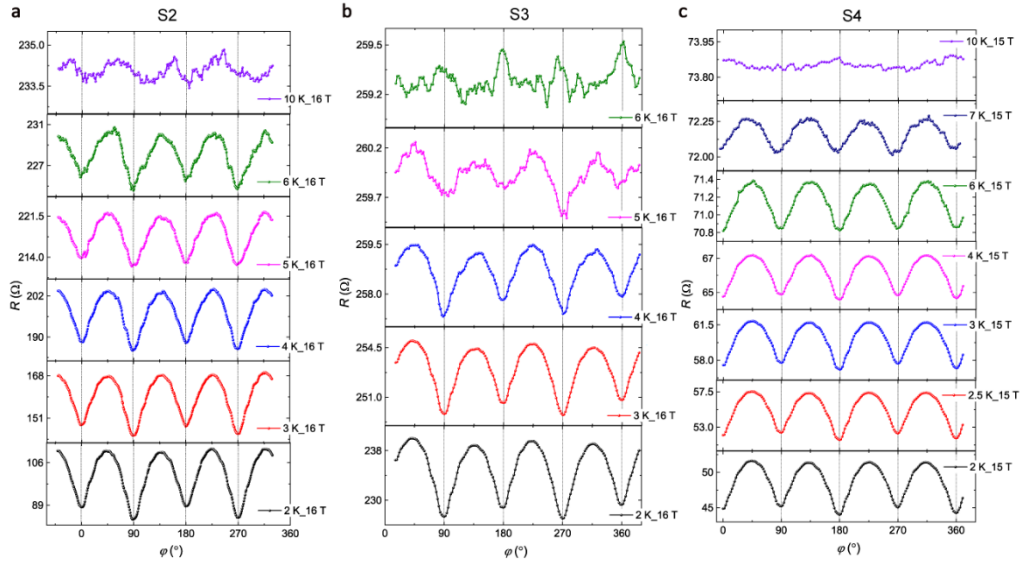


Fig. S13. Reproducible C_2 anisotropy superimposed on the C_4 symmetry in more samples. $R(\varphi)$ at different temperatures under 16 T from sample S2(a), S3(b), and S4(c), showing both the reproducible C_4 and C_2 symmetric features. The C_4 anisotropy is manifested as four minima at 0° , 90° , 180° , and 270° (maxima at 45° , 135° , 225° and 315°) (a, b and c). The C_2 anisotropy is manifested as $R(0^\circ)$ being larger than $R(90^\circ)$ (a) or $R(0^\circ)$ being smaller than $R(90^\circ)$ (b and c). The observations are consistent with the results of S1 shown in the main text.

References

36. Jovanović, V. P., Fruchter, L., Li, Z. Z., Raffy, H. Anisotropy of the in-plane angular magnetoresistance of electron-doped $\text{Sr}_{1-x}\text{La}_x\text{CuO}_2$ thin films. *Phys. Rev. B* **81**, 134520 (2010).
48. Hamill, A. et al. Two-fold symmetric superconductivity in few-layer NbSe_2 . *Nat. Phys.* **17**, 949-954 (2021).